International Journal of Hydrogen Energy 204 (2026) 153254

Contents lists available at ScienceDirect

International Journal of Hydrogen Energy

journal homepage: www.elsevier.com/locate/he

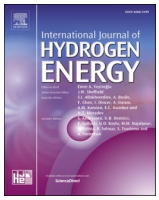

Simulation of flame development in a glass furnace with hydrogen enriched natural gas

Carlo Cravero, Davide Marsano *, Gabriele Milanese

Dipartimento di Ingegneria Meccanica, Energetica, Gestionale e dei Trasporti (DIME), Università degli Studi di Genova, Via Montallegro 1, 16145, Genova, Italy

ARTICLE INFO

Keywords:
Combustion
Hydrogen
Glass furnace
CFD
Coupling

ABSTRACT

The glass manufacturing industry is energy demanding and has significant environmental impacts due to the high temperatures required for melting raw materials, resulting in pollutant emissions. With the EU's goal of climate neutrality by 2050, reducing energy consumption and emissions in glass production is a key priority. Integrating some quantities of hydrogen in the fuel mixture can offer a promising solution for decarbonization. While hydrogen is being explored in industries like steel, its potential as a clean fuel for glass furnaces still requires further research. This study focuses on the impact of introducing hydrogen into the fuel mixture for glass furnace combustion. Using an innovative CFD framework that overcomes the limitations of existing models—where combustion is typically treated with oversimplified approaches and the glass tank is solved separately via iterative coupling between domains—this work introduces a fully coupled simulation of both the combustion space and the glass bath within a single computational environment. The reactive flow is resolved using a reduced chemical kinetic mechanism in combination with the EDC (eddy dissipation concept) turbulence–chemistry interaction model, enabling an accurate representation of combustion development. This advanced setup is employed to assess the effect of hydrogen enrichment while maintaining the same overall thermal input power as the natural-gas-only baseline case. The results demonstrate that a 30 % hydrogen addition (by energy) can achieve a substantial reduction in CO_2 emissions of nearly 30 % and a decrease in NO emissions of approximately 40 %, highlighting the significant environmental benefits of hydrogen enrichment, while simultaneously introducing serious flame stability challenges that must be carefully managed. This behaviour has been thoroughly analyzed, with particular focus on flame patterns, heat flow distribution and glass surface temperature. To address this challenge, some strategies are proposed to stabilize combustion, restoring stable flame conditions akin to those observed with natural gas. The study aims to explore hydrogen's potential in decarbonizing the glass industry, offering practical solutions for integrating hydrogen into production processes with promising results. This contributes to reducing industrial carbon emissions and supports the transition to a more sustainable energy system.

1. Introduction

The glass manufacturing industry is one of the largest production sectors, with significant impacts on other sectors, including automotive, construction and consumer goods. It provides essential materials for products such as windows, containers and bottles. The efficiency of glass production plants is crucial for their long-term sustainability, making them distinct from other industries like plastics. A major challenge in glass production is the significant energy required to melt the raw materials, because furnaces are energy intensive process reaching temperatures around 1600 C; moreover, they emit considerable amounts of CO_2, NO_x and SO_x into the atmosphere. In 2022, global glass production reached approximately 150 million tons, with about 40 % of this being flat glass (used in construction, automotive, electronics, etc.) and 47 % being hollow glass (including containers and bottles) [1]. In Europe, total glass production amounted to 39.5 million tons in 2022, underscoring the region's continued prominence in the industry; In particular, Italy is the second largest glass producer in Europe. The European glass industry consumes approximately 8 GJ of energy per ton of production annually [2]. This sector is responsible for about 22 million tons of CO_2 emissions per year in Europe. It is estimated that the natural gas consumption in this sector exceeds 1 billion cubic meters annually [3]. The

* Corresponding author.
E-mail address: davide.marsano@unige.it (D. Marsano).

https://doi.org/10.1016/j.ijhydene.2025.153254
Received 17 June 2025; Received in revised form 23 December 2025; Accepted 26 December 2025
Available online 30 December 2025

recent European Green Deal introduced a set of measures designed to make the Union's economy sustainable, promote efficient resource use, and reduce pollution. The European Union aims to achieve climate neutrality by 2050, and to reach this goal, it plans to decarbonize its industrial sectors [4]. Given this global context to reduce energy use and greenhouse gas emissions, optimizing glass production processes has become a crucial goal.

Modern continuous glass furnaces are complex thermal-fluid systems that involve a variety of physical phenomena. These include the conversion of batch materials into molten glass, radiation within the molten glass, natural convection driven by buoyancy forces, joule heating from AC electrodes, turbulent combustion and the thermal coupling between the combustion environment and the glass bath. More specifically, a typical glass furnace consists of a combustion chamber and a glass tank, where the turbulent, diffusive flames from the combustion space transfer energy to the tank, mainly through radiation. Enhancing the efficiency of this energy transfer presents an opportunity to reduce both energy consumption and emissions, making it a critical area for innovation in the quest for more sustainable glass manufacturing. Raw materials are fed into the glass tank, where they undergo chemical reactions, melting and homogenization over a period of several hours before exiting the furnace. Various strategies have been developed to minimize the environmental impact of glass production. These include the implementation of regenerative or recuperative chambers [5,6], systems for pre-heating raw materials [7], exhaust gas recirculation techniques [8] and air staging methods to lower specific emissions, such as NOx [9,10]. Additionally, advancements in glass bath technology have led to the integration of boilers [11] and electrodes [12], which enhance the homogenization process and improve quality while reducing thermal energy consumption.

An additional solution to support decarbonization in industrial production is the use of low carbon fuels as replacements for conventional fossil fuels or renewable energy. Biogas, synthetic methane and green hydrogen all meet these requirements. Among these, hydrogen stands out as the most promising clean fuel, offering high calorific value, good thermal conductivity and a high reaction rate. In the iron and steel industry, hydrogen use is already being explored [13–15]. Similarly, in the glass industry, hydrogen is being considered as an alternative energy carrier for combustion. However, this requires extensive research to ensure a smooth transition, taking into account existing plants and the infrastructure of national gas pipelines. Recently, projects such as HyGlass [16], HyNet [17], and Kopernikus P2X [18] have been launched. In this initial phase, introducing small amounts of hydrogen into the gas pipeline network is relatively easy to implement, with a blend of up to 20 % by volume already being achieved; larger volumes are expected to be introduced in the near future [19]. However, it is crucial to study the impact on combustion and the potential response of the glass furnace, which is designed to ensure the proper quality of molten glass based on convectional practices, when using such a fuel mixture.

Some studies in the literature have explored combustion with hydrogen blends in simpler test cases. Lee et al. [20] found that higher hydrogen content in fuel blends increased heat release, combustion pressure, and burning velocity, while reducing unburnt hydrocarbons and CO_2 emissions but raising NO_x levels. Ozturk et al. [21] showed that a 0.3 hydrogen blend improved energy efficiency by 4.4 % and reduced CO_2 emissions by 20.87 %. Furthermore, several numerical studies have used models to characterize the combustion properties of various hydrogen blends. Flamelet models were applied to swirl burners with hydrogen blends up to 30 % [22,23]. Ziani [24] tested a modified k-epsilon model with a flamelet approach on a jet burner for hydrogen blends up to 50 %. Additionally, Eddy Dissipation Models were applied to swirl burners with different blend ratios [25,26]. These studies highlighted how the flame structure, including ignition, stability, and length, varied depending on the hydrogen content, in addition to changes in emissions and energy release.

Due to the complexity of the physical mechanisms involved in a glass furnace, it is essential to model the system accurately. Numerical studies on this topic have been available in the literature since the 1980s, starting with the introduction of simplified 3D furnace models [27,28]. Carvalho [29] developed a detailed furnace model with sub-models specifically for the combustion space, glass tank, and batch blanket. This foundational work laid the groundwork for many subsequent advancements, particularly in the development of glass bath modelling [30–39]. Recent studies have focused on 3D simulations of glass furnaces using commercial software. Abbassi and Khoshmanesh [40] modelled and validated a side-port glass furnace, dividing it into key components (combustion chamber, batch blanket, and glass tank) using Gambit/Fluent. Li et al. [41] used Glass Service software to simulate the combustion chamber of a glass bath in 3D. Raic et al. [42] and Daurer et al. [43] explored oxy-fuel glass furnaces using Ansys Fluent. These studies reflect ongoing efforts to improve the understanding and optimization of glass furnace processes.

Previous CFD studies on glass furnaces typically rely on simplified combustion models (such as Flamelet or global kinetic schemes) to reduce computational cost and they treat the combustion space and the glass tank as separate domains coupled through iterative procedure. This modelling strategy introduces several critical limitations: simplified kinetics fail to reproduce the real interplay between fuel, oxidizer and combustion products, leading to inaccurate flame structure and heat release patterns; moreover, solving the two domains sequentially prevents a truly simultaneous exchange of heat flow and temperature. As a consequence, temperature and heat flow fields become inconsistent across the interface and multiple coupling iterations are required to reach convergence, often without fully capturing the real thermo-fluid dynamics of the furnace.

The research group has made significant progress in developing fluid dynamic models to simulate and assist in the design of various components in glass production plants [44–47]. In terms of combustion, they have validated combustion models using a well-established test case from the literature [48]. Building on this experience, the team developed an accurate CFD model to simulate a real glass furnace. In this model, a reduced kinetic mechanism was applied in the combustion chamber, combined with the EDC turbulence–chemistry interaction model. Additionally, a full coupling of the combustion space and the glass tank was implemented, enabling the simultaneous simulation of both domains and ensuring consistency between the heat flow and temperature distributions on the glass surface [49,50].

In this work, the furnace model developed was applied to simulate the introduction of a certain amount of hydrogen while keeping the global input thermal power constant compared to the base case using only natural gas. The goal was to analyse the impact of adding hydrogen to the fuel mixture on the development of combustion within the combustion space. The furnace and the numerical model used for the simulations were first described in detail. After a brief model validation, already extensively demonstrated in previous work [50], the results showed how the hydrogen addition can lead to reduced combustion stability with the development of a specular, twin-flame patterns. This behaviour has been thoroughly investigated and explained. Given this issue, different strategies were investigated to restore a stable flame pattern similar to that observed in the base case with natural gas only.

This work introduces a fully coupled CFD modelling framework that simultaneously resolves the combustion chamber and the glass bath, representing a substantial advancement over conventional simulation strategies that treat these domains separately and often result in inaccurate predictions of flame structure, heat release and thermal interaction with the melt. By solving the two domains in a unified and thermally consistent manner, the proposed approach overcomes intrinsic limitations of segregated methodologies and enables a more realistic representation of furnace operation. Combustion is modelled through a reduced chemical kinetic mechanism coupled with the Eddy Dissipation Concept (EDC) turbulence–chemistry interaction model,

providing an optimal balance between physical fidelity and computational efficiency under industrial-scale conditions.

Within this novel fully coupled framework, the model is employed to systematically investigate the effects of varying hydrogen enrichment levels on flame characteristics, heat transfer and overall furnace performance. The primary objective of this study is to quantitatively assess the decarbonization potential of glass furnaces using a comprehensive, physics-based CFD tool. By focusing on hydrogen as a low-carbon fuel, this work aims to identify viable transition pathways and to deliver actionable insights that can support the glass industry in its shift toward sustainable and low-emission energy solutions.

2. Plant layout

This research investigates the simulation of a glass manufacturing facility specifically tailored for producing pharmaceutical-grade borosilicate glass. The furnace operates as a gas-fired, with recuperative capabilities, designed to operate with an end-port configuration that minimizes space requirements, making it highly efficient and compact. The combustion chamber features the consolidated arc-shaped crown, which optimizes the distribution of heat within the furnace. Additionally, it is equipped with two air vents, each of them housing two separate burners. The burners are mounted in specially designed conical burner ports. This configuration provides several technical advantages. The conical geometry ensures a precise alignment of the fuel and oxidizer jets into the combustion chamber, promoting stable flame attachment and optimal mixing. Additionally, this design allows burners to be quickly replaced or interchanged, including with burners of different diameters, without requiring a furnace shutdown. These burners are responsible for generating two distinct primary flames that operate concurrently, ensuring a stable and consistent heat source for the glass melting process. The fuel mixture enters through fuel jets at the ambient temperature. At the same time, pre-heated air from the recovery chamber is channelled into the furnace through the two air vents, helping to sustain the combustion process. Notably, the air-to-fuel ratio is carefully controlled to maintain the optimal balance between air and fuel; the operating conditions can be adjusted to ensure efficient combustion, improve energy efficiency, reduce pollutant emissions and regulate the furnace temperature. The exhaust gases generated during the process are expelled through a single port located above the two air vents, allowing for the safe and efficient removal of combustion products.

The glass tank, which is specifically designed for the production of small volumes of molten glass, operates with a carefully controlled raw material feeding system. The materials are introduced into the tank through a single doghouse located on the right side. This feed includes a certain proportion of recycled glass material, which enters at ambient temperature, contributing to both the sustainability of the process and the quality of the final product. Due to the plant's specialized design and compact layout, the batch blanket is confined to a relatively small area near the doghouse. This localized batch blanket setup helps optimize the heating process and ensures that the raw materials are evenly distributed across the tank, thereby improving energy efficiency. To further enhance the control over the glass melting and refining processes, a split wall is strategically positioned along the tank floor, approximately two-thirds of the tank's total length. This barrier effectively separates the melting zone from the refining zone, ensuring that the molten glass undergoes the necessary processes to reach the desired quality and consistency. Although the tank is equipped with electrodes and boilers to facilitate additional heat and energy control, these components are not currently in use. However, their design offers the potential for future operational flexibility, should the need arise to adjust or optimize the production process further.

For the purposes of this research, various operating conditions of the furnace were considered. First, compared to the baseline case using only natural gas, the addition of hydrogen to the fuel mixture was tested while maintaining the same thermal energy input. A hydrogen energy contribution of 30 % was examined, which corresponds to approximately 60 % in terms of mole fraction. Initial analyses were conducted with the air-to-fuel ratio kept constant, specifically with a 5 % air deficit. Subsequently, the operating conditions were varied by adjusting the air-to-fuel ratio, while the amount of fuel supplied remained unchanged.

Fig. 1 shows the schematic layout of a recuperative glass furnace.

It should be noted that the detailed furnace geometry is subject to a non-disclosure agreement with the industrial partner. For the same reason, the numerical values of the CFD model inputs are not explicitly reported in the following sections.

3. Mathematical model

3.1. Combustion space

The development of combustion is highly complex, influenced by the interactions between chemical reactions, turbulence and radiative heat transfer. The models employed to capture these phenomena are briefly described below.

The mathematical problem has been described in more detail in a previous work [50]. It is based on the Reynolds-averaged Navier–Stokes equations, where the mass, momentum and total energy balance equations are considered.

The turbulence closure adopted is the standard k-ε model [51,52], using standard wall functions. This model is well-regarded for its robustness and numerical stability, particularly when dealing with turbulent jets and reactive flows in industrial applications [53]. All the model coefficients are set in accordance with Jones and Launder [54]. The two turbulent scales K and ε are obtained by solving the corresponding transport equations:

$$\frac{\partial \overline{\rho} K}{\partial t} + \overline{u}_i \frac{\partial \overline{\rho} K}{\partial x_i} = -\overline{\rho u_i' u_j'} S_{ij} + \left(\mu + \frac{\mu_T}{\sigma_k}\right) \frac{\partial K}{\partial x_i} - \overline{\rho}\varepsilon \tag{1}$$

$$\frac{\partial \overline{\rho} \varepsilon}{\partial t} + \overline{u}_i \frac{\partial \overline{\rho} \varepsilon}{\partial x_i} = -c_{\varepsilon 1} \frac{\varepsilon}{K} \overline{\rho u_i' u_j'} S_{ij} + \frac{\partial}{\partial x_i}\left(\mu + \frac{\mu_T}{\sigma_\varepsilon} \frac{\partial \varepsilon}{\partial x_i}\right) - c_{\varepsilon 2} \overline{\rho} \frac{\varepsilon^2}{K} \tag{2}$$

where the Reynolds stress tensor $\overline{\rho u_i' u_j'}$ is modelled with Boussinesq-type approximation and S_{ij} is the rate of strain tensor while the turbulent viscosity (μ_t) is computed by combining the turbulent kinetic energy (K)

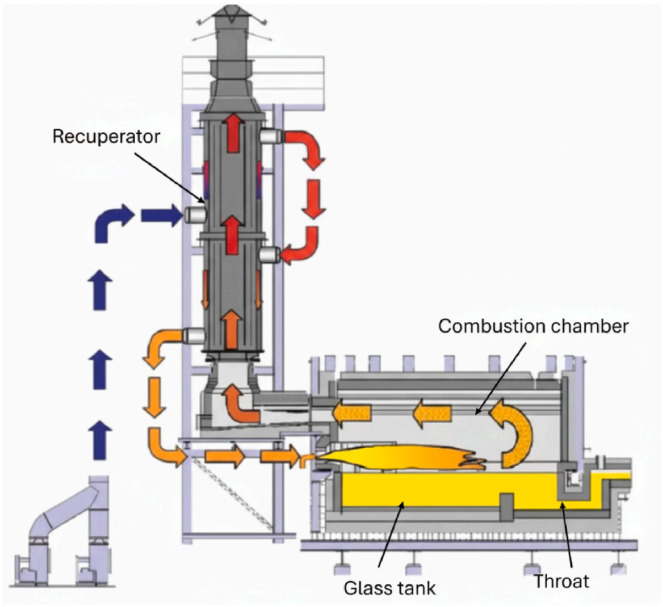

Fig. 1. Schematic layout of a recuperative glass furnace.

and its dissipation rate (ε):

$$\mu_t = C_\mu \rho \frac{K^2}{\varepsilon} \tag{3}$$

The Radiative heat transfer is calculated using the P1 model, a simplified version of the radiation transport equation that assumes isotropic radiation intensity [55]. This model is combined with the weighted-sum-of-grey-gases model (WSGGM) to capture the effects of spectral gas absorption.

Furthermore, the composition of chemical species is determined by solving the relevant transport equations, expressed in the following form:

$$\frac{\partial}{\partial t}(\overline{\rho Y_n}) + \frac{\partial \overline{\rho Y_n u_j}}{\partial x_j} = -\frac{\partial \mathbf{J_n}}{\partial x_j} + R_n \tag{4}$$

Where R_n is the net rate of production of species *n* by chemical reactions and $\mathbf{J_n}$ is the sensible enthalpy. Specifically, N-1 species transport equations are solved, with N denoting the total number of chemical species present in the system.

The Eddy Dissipation Concept (EDC) model is employed to account for the interaction between turbulence and chemical reactions, which are assumed to take place within the small turbulence structures [53,56,57]. The volume fraction of fine scales and the reaction time scale are modelled using the length scale (γ*) and the mean residence time (τ*), as reported in the following relationship:

$$\gamma^* = C_\gamma \left(\frac{\nu\varepsilon}{K^2}\right)^{1/4} \tag{5}$$

$$\tau^* = C_\tau \left(\frac{\nu}{\varepsilon}\right)^{1/2} \tag{6}$$

To accurately represent the combustion process, the DRM 19 chemical kinetic mechanism is used [58,59]. This reduced mechanism, derived from the detailed GRIMECH model, includes 19 species and 84 reversible reactions, along with the associated thermodynamic and transport properties. Further details of the chemical kinetic mechanism can be found in previous studies [48].

For NO prediction, solving the detailed chemical kinetics (DCK) for NOx formation is very demanding because it involves a large number of reactions, especially in large domains. To overcome this limitation, the Chemical Reactor Network (CRN) approach is commonly adopted. In this method, the DCK solution, whose computational cost is typically too high for direct CFD simulations of industrial systems, is obtained by solving only the species balance equations on a CRN that corresponds to the CFD-simulated flow domain. Advection, diffusion and (usually) temperature fields are taken directly from the CFD results and kept fixed, while the reaction rates are evaluated using the detailed kinetic mechanism [60]. The simplest form of a CRN can be derived directly from the CFD mesh [60–62], by treating each computational cell as a Perfectly Stirred Reactor (PSR) [63]. This approach is consistent with the standard CFD practice of computing reaction rates via Arrhenius expressions, as in laminar combustion modelling [64]. In this work, a procedure similar to that of Skjøth-Rasmussen et al. [60] was implemented within the ANSYS Fluent solver. The same computational mesh used for the thermo-fluid-dynamic simulations was employed, but the reduced kinetic scheme used in the first step was replaced with a detailed mechanism to predict NOx emissions. In this second step, the thermo-fluid-dynamic fields are not updated, as is typical of other reactor-network-based post-processing methods.

The in-situ adaptive tabulation (ISAT) method is employed to enhance computational efficiency. The method's accuracy was verified by comparing results obtained with a tolerance reduced by two orders of magnitude, showing minimal deviation. The fluid mixture is treated as an incompressible ideal gas, with mixture-specific heat, molecular viscosity and thermal conductivity determined using the mixing law. Mass diffusivity is computed based on kinetic theory, ensuring consistency with fundamental transport principles. This model was developed and validated through a series of simulations on literature test cases, as detailed in previous works [48,50].

3.2. Glass tank

The flow of molten glass, primarily influenced by free convection cells, was simulated as laminar flow; this assumption is justified by the relatively low velocities of the molten glass and the high viscosity of the material, which result in low Reynolds numbers throughout the flow domain. Then, in the molten glass domain, radiative heat transfer was not modelled explicitly. Instead, its contribution was accounted for by adopting an equivalent thermal conductivity [35,40], increased with respect to the purely conductive value. This modelling strategy is justified by the fact that molten glass behaves as a semi-transparent medium in which radiative transfer occurs mainly through short-range absorption and re-emission mechanisms. Numerous studies have shown that, under such conditions, radiation effects can be lumped into an enhanced conductivity term, providing an accurate representation of the overall heat transport without the computational cost associated with solving the radiative transfer equation within the glass bulk, where radiation effects were not included in the analysis.

So, the simulation was carried out by solving the mass, momentum and energy equations to capture the fluid dynamics. To account for the temperature-dependent behaviour of the glass, its properties were modelled to vary with temperature, using either step functions or polynomial relations within the relevant temperature range. In addition, the dynamic viscosity of the molten glass was represented by an expression that incorporates both the temperature and the chemical composition of the glass [50]. This expression is specific to the production plant in question, reflecting the unique characteristics of the glass composition and the operating conditions within this facility. The relationship between viscosity, temperature and composition plays a crucial role in accurately modelling the flow behaviour and ensuring a realistic simulation of the molten glass flow under various conditions.

4. CFD model

The computational domain spans both the combustion chamber and the molten glass bath, with each region discretized using an unstructured mesh of tetrahedral elements, created using Ansys ICEM CFD v. 17.1. The combustion chamber, which includes the air and exhaust vents, as well as the fuel burner housings, was meshed with varying densities to accurately capture the complex flow characteristics. In areas near the walls, where boundary layer effects are most significant, the mesh was refined with prism layers to maintain a y + value of approximately 30. This refinement ensures that the wall functions are properly activated, allowing for more accurate representation of the flow and heat transfer near the surfaces.

In the molten glass bath, the mesh was designed to align the elements at the glass surface with those in the regions above. This alignment is crucial for accurately capturing the thermal gradients and flow dynamics between the two regions. Starting from the free glass surface, additional prism layers were incorporated to precisely capture the temperature variations and flow behaviour within the molten glass. The combustion chamber mesh contains roughly 4 million elements, while the glass bath mesh consists of about 2 million cells. These mesh sizes were determined through a detailed mesh sensitivity analysis conducted in previous studies [44,46,48,50], which ensured that the grid resolution was sufficient to obtain reliable results while maintaining computational efficiency. Fig. 2 shows the surface mesh of the two computational domains, with the mid-height line along the superstructure superimposed, corresponding to the location where the temperature measurements were compared.

The steady simulations were carried out using the finite volume

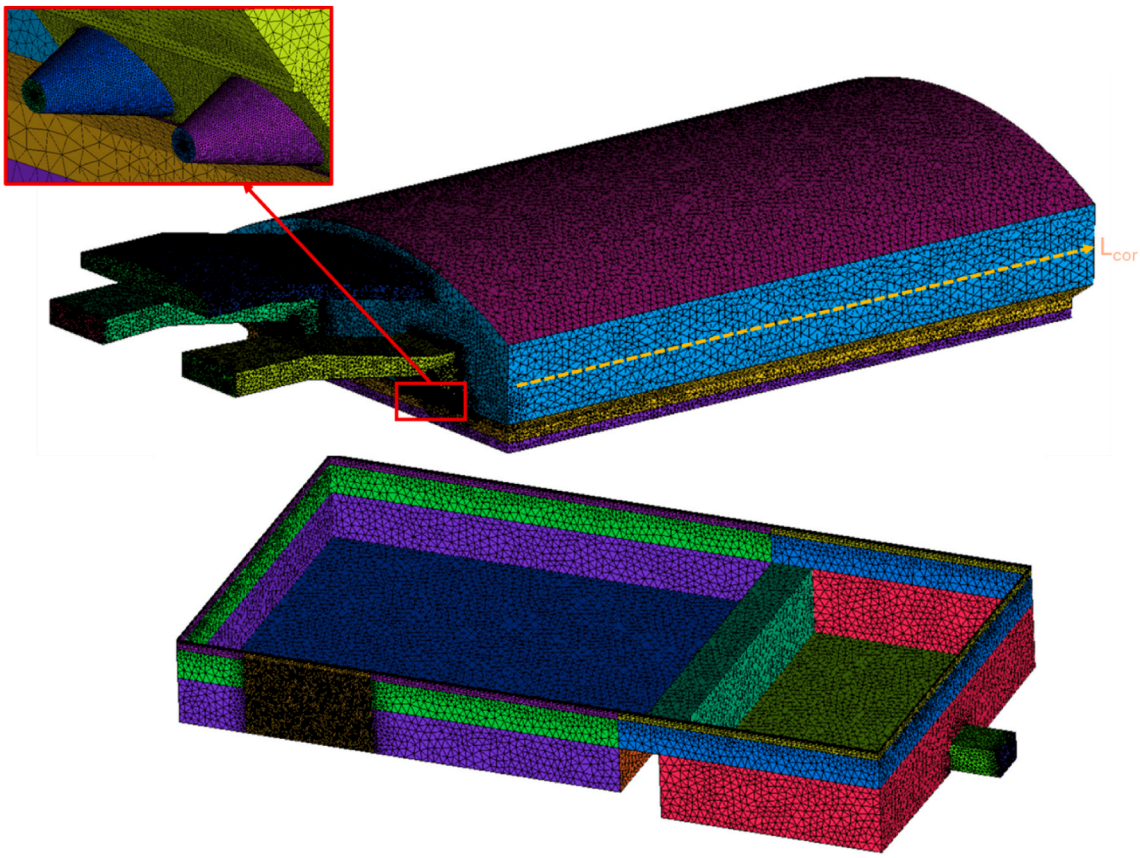

Fig. 2. Computational grids of the combustion space and glass tank.

method within the ANSYS Fluent 17.1 environment [64]. A pressure-based solver was employed, with a coupled scheme for pressure-velocity coupling, which is known to provide stable and accurate results for a wide range of fluid flow problems. The advection terms were discretized using a second-order upwind scheme, which offers higher accuracy in capturing the convective transport of quantities such as heat, momentum, and species. To ensure that the numerical solution converged properly, multiple criteria were used to monitor the solution progress. Residuals, monitor points, and global balances were tracked throughout the simulation. Specifically, monitoring points were strategically positioned along the fuel jet axis to track key flow variables, including temperature, velocity, and O_2 mole fraction. These points play a crucial role in verifying the stability of the solution and ensuring that the flow dynamics are accurately resolved, particularly in regions of interest where strong gradients in temperature and species concentration are expected. A slight instability persists on the combustion side, which is commonly observed when performing steady RANS simulations of inherently unstable flows [65,66]; this effect is further amplified by combustion processes, as also reported in real furnace conditions [41]. However, the convergence achieved at these monitoring points, together with the overall global balance checks, confirms the accuracy and reliability of the simulation results.

4.1. Boundary conditions

In the combustion chamber, air was introduced uniformly through the air vents, with a fixed preheated temperature. At the burner inlets, a fuel mass flow rate, was supplied at ambient temperature. Several cases were simulated, each with a different fuel composition to incorporate hydrogen (H_2), while maintaining the same thermal energy content as the baseline case. The exhaust gas outlet was assigned an atmospheric pressure condition to reflect the natural discharge of gases from the furnace. The furnace walls were modelled as no-slip boundaries, with heat flow values provided by the glass producer applied at various surface patches, along with a constant emissivity (ε_v) value of 0.8 to account for radiative heat transfer. This value, provided by the industrial partner, is consistent with typical emissivity ranges for alumina- and silica-based refractories at high temperatures. Furthermore, previous validation work [50] has confirmed that this assumption yields accurate predictions of radiative heat transfer within the furnace. At these temperatures, variations due to surface roughness or minor material differences are negligible, making a constant emissivity of 0.8 a reasonable and well-supported approximation for the CFD simulations.

For the glass bath inlet, the flow rate of glass raw material was set to match the daily production output of the reference furnace, while the temperature was specified to be at ambient conditions. A corresponding outlet condition was applied at the throat of the glass tank to simulate the natural flow of the molten glass. The lateral walls and furnace floor were also modelled as no-slip boundaries, with an outgoing heat flow applied to reflect the thermal energy leaving the system. To account for the thermal energy required for the chemical processes (i.e. the fusion) involved in glass melting, as well as the precise amount of recycled material being incorporated into the process, a uniform negative heat source was included within the domain. This heat source was carefully calibrated to reflect the energy absorption necessary for the reactions taking place in the furnace, ensuring that the model accurately represents the real-world conditions of the glass production process.

4.2. Coupling of combustion space to glass tank model

The methodology adopted in this study is designed to achieve a comprehensive coupling between the combustion chamber and the molten glass bath, ensuring that there is consistency in the heat flow and temperature distribution on the free glass surface. The approach consists

of several distinct phases. In the initial phase, the two domains, the combustion chamber and the glass bath, are solved independently to establish appropriate initial conditions for the coupled simulation. During these preliminary simulations, the boundary condition at the free glass surface is derived from the solution obtained in the adjacent domain. This provides a realistic starting point for the next phase. The final step involves simultaneously solving both domains thermally coupled through an interface, starting from the results of the previous simulations. This phase enables full thermal coupling between the two regions.

Each domain evolves according to its own characteristic time, which is especially beneficial since the time scale of the glass bath is significantly longer (hours) than that of the reactive flow in the combustion chamber (milliseconds). The proposed strategy was preliminarily assessed on simplified configurations consisting of two domains characterized by distinct thermophysical properties and flow conditions. Starting from independent initial solutions, the coupling procedure allowed the two regions to reach a consistent thermal state within acceptable computational times. As a result, the global heat balance of the furnace is correctly established, yielding a temperature and heat flux distribution at the glass surface that naturally reflects the interaction between combustion phenomena and convective motions.

Additional details are provided in previous works [49,50].

5. Results

5.1. Validation

The validation of the adopted CFD model was previously carried out in a prior study on the same furnace [50], focusing on the case with only natural gas, for which existing experimental data were available. Specifically, the validation was conducted by comparing the numerical values obtained from the CFD simulation with experimental data from thermocouple, such as the temperature at the superstructure, the temperature of the molten glass at the throat and the oxygen concentration in the exhaust gases. For instance, Fig. 3 shows the numerical temperature distribution along both the right and left superstructures. The comparison with experimental data is performed at mid-height of the wall, where the thermocouples are installed; the corresponding measurement locations are indicated by the discrete points shown in Fig. 2. The simulation results closely match the experimental data, effectively capturing the overall temperature trend. The maximum deviation observed is approximately 1.5 %.

Additionally, the power balance was shown to be consistent across both positive and negative energy terms, thanks to the simultaneous resolution of both the combustion chamber and the glass tank, made possible by the innovative fully thermal coupled approach. The combustion model employed in this work has been previously assessed in studies concerning CH_4 diffusion flames under high-temperature oxidizing conditions [48] and in simulations of the IFRF experimental furnace [67]. Such prior validation is of particular importance, as conducting comprehensive measurements within industrial glass furnaces is experimentally challenging. As a consequence, large-scale furnace evaluations are generally restricted to thermocouple readings at selected locations, which also represents the approach adopted in the present study. On the basis of the demonstrated robustness of the combustion model, a novel thermal coupling strategy is implemented, specifically designed to address the oversimplifications commonly encountered in earlier methodologies. This enhancement provides a more stringent framework for evaluating the overall fidelity of the CFD simulation.

5.2. Analysis of the hydrogen addition to the fuel mixture

The analysis begins by examining how the flame patterns inside the glass furnace is influenced by the introduction of hydrogen into the fuel mixture, while maintaining a constant thermal power input. This study was conducted under the assumption that the furnace configuration remained unchanged, meaning the burner geometry, layout and operational conditions were held constant. The aim was to isolate the effect of hydrogen addition on the flame behaviour and flow dynamics. Fig. 4 shows a volume rendering of OH mass fraction (the primary indicator of the flames structures) for two scenarios: the baseline configuration with natural gas as the fuel and the configuration in which 30 % of the thermal power is supplied by hydrogen.

The visualizations reveal the development of the diffusive flames generated by the interaction between preheated combustion air from the two towers and the fuel jet from the burners. The comparison of the two cases shows significant differences in flames structure. In the hydrogen-enriched case, the slight instabilities observed on the combustion side in the baseline scenario become more pronounced. Specifically, the numerical solution identifies two main, specular flame patterns: the right-side flame is well-developed while the adjacent left flame appears distorted (FP_1); conversely, the left-side flame becomes dominant, with the right flame exhibiting distortion (FP_2). In practical terms, one flame tends to develop predominantly along the axial direction, while the adjacent flame bends and converges toward it. This alternating pattern suggests a likely cyclic and asymmetric flame behaviour, indicating a reduced combustion stability in the combustion chamber when

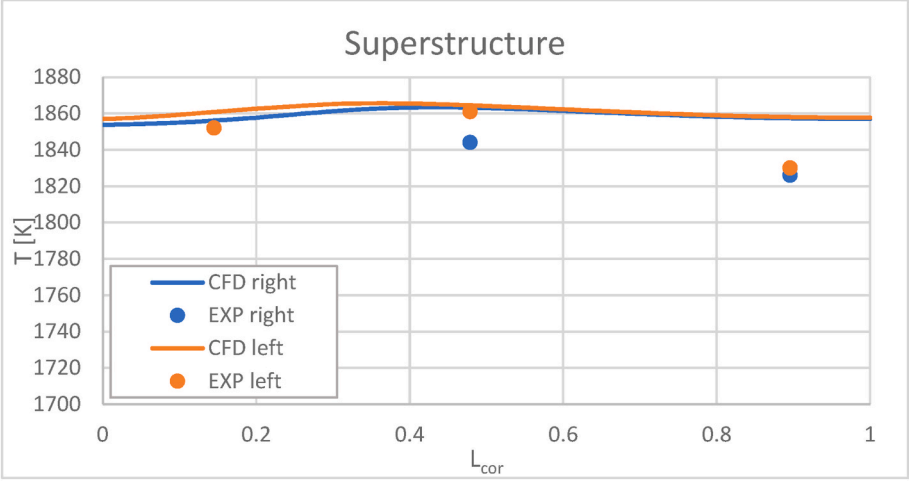

Fig. 3. Comparison of the numerical temperature distribution on the right (in blue) and left (in orange) superstructure walls against the experimental measurements. (For interpretation of the references to colour in this figure legend, the reader is referred to the Web version of this article.)

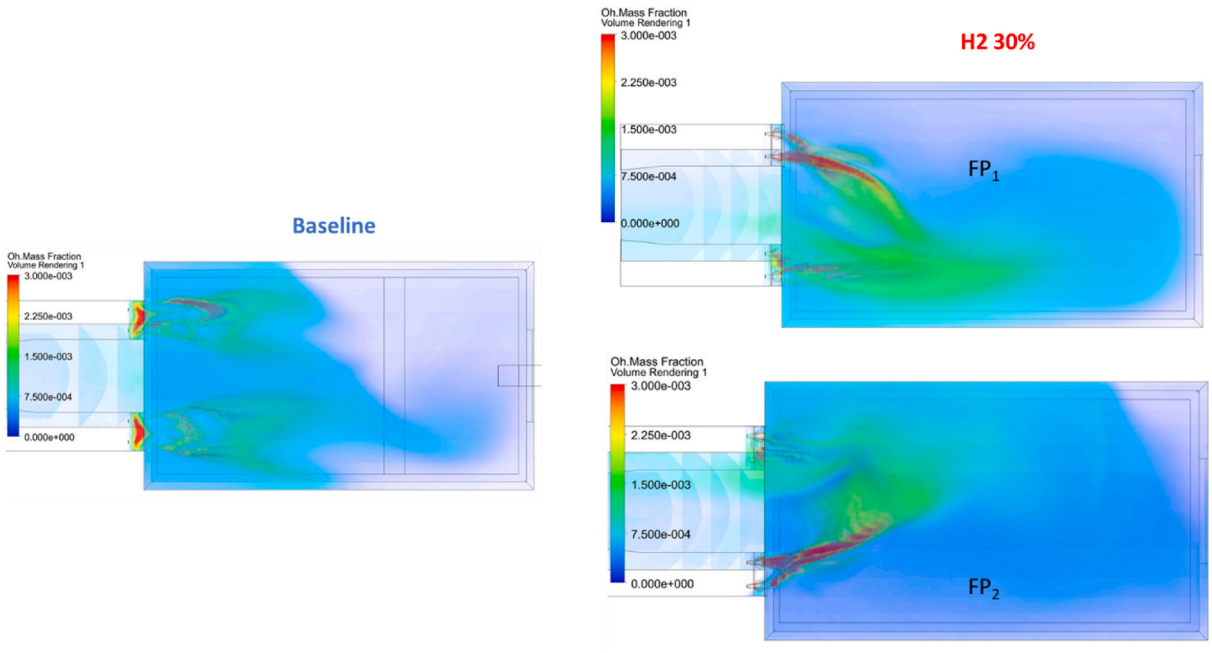

Fig. 4. Comparison of OH volume rendering in the combustion chamber between the baseline case (on the left) and the 30 % H_2 case (on the right, different flame patterns).

hydrogen is introduced into the fuel mixture for this type of glass furnace. Another notable difference lies in the geometric characteristics of the flames. In the hydrogen-enriched case, the flames are narrower and more elongated, particularly the dominant axial flame, compared to the baseline configuration. In contrast, the flames in the baseline configuration exhibit greater radial spreading, contributing to a more diffuse and stable flame structure. The introduction of hydrogen not only alters the flow dynamics, but also influences the spatial distribution and morphology of the flames. Additional analyses were carried out on fuel mixtures with 15 % hydrogen enrichment in terms of energy performance, showing comparable stability. These results are not reported here for the sake of conciseness, as they would not substantially increase the added value of the discussion. The investigation was therefore continued directly with the 30 % hydrogen case, which was selected by the industrial partner for forthcoming experimental testing.

From these solutions, it is evident that introducing hydrogen can significantly alter the flame structure and stability. The two main flame patterns identified, combined with the narrower and more elongated shape of the dominant flame, set potential challenges for maintaining a more stable combustion in the glass furnace under these conditions. This highlights the need for further investigation into burner design and operational strategies to mitigate this behaviour and fully exploit the

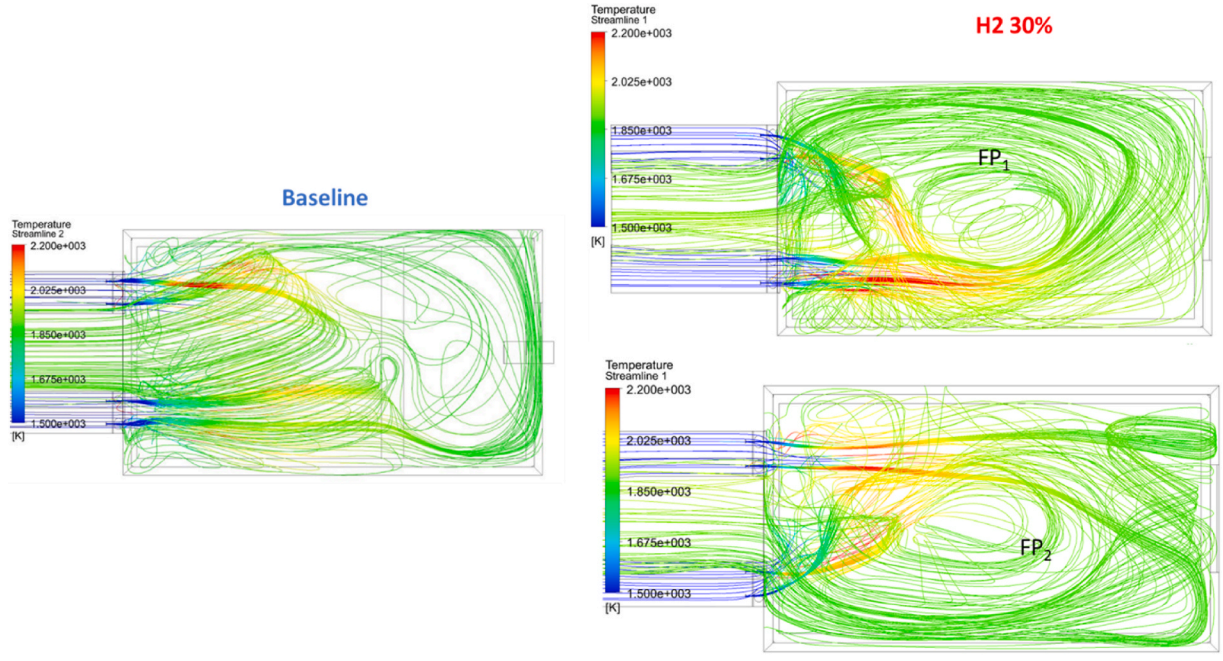

Fig. 5. Comparison of streamlines in the combustion chamber originating from the air vents and burners, between the baseline case (on the left) and the 30 % H_2 case (on the right, different flame patterns).

potential benefits of hydrogen as a fuel.

To further investigate the mechanisms underlying these differences in flame patterns, Fig. 5 displays the streamlines generated from the air vents and burners for both configurations. These streamlines are coloured by temperature to provide additional insight into the interaction between the flow field and the thermal characteristics of the system. These visualizations capture the flow patterns driven by combustion, providing valuable insights into the structure of the flames.

In the baseline case, a recirculation pattern is clear along the back wall, characterized by a flow returning toward the exhaust gas port (positioned higher than the two air vents). In this configuration, the exhaust gases have only a lower influence on the flame structure, allowing the two flames to develop in a parallel manner without significant interference. In contrast, in the hydrogen-enriched case, the influence between the flames and the combustion products returning towards the exhaust tower becomes much more pronounced. Specifically, one flame develops dominantly in the axial direction, while the high-velocity exhaust gases, after rebounding off the front wall, modify the trajectory of the adjacent flame, causing it to deviate. This phenomenon occurs because in the hydrogen-enriched configuration, the flame tends to ignite earlier than in the natural gas case; in addition, the flame appears to spread less in the radial direction while becoming longer axially.

Fig. 6 provides a detailed view (zoomed-in) of the volume rendering of OH mass fraction and the streamlines, coloured by temperature, in the mixing region for both configurations. This visualization highlights the differences in flow behaviour and flame development between the baseline and hydrogen-enriched scenarios, offering further insight into the interplay between exhaust gas dynamics and flame structure.

From this visualization, the earlier ignition in the hydrogen-enriched case becomes clear. Additionally, it can be observed that the distorted adjacent flame tends to pass over the well-developed dominant flame. This behaviour occurs because the exhaust gases from the dominant flame, in their return path, flow outward along the lateral walls and subsequently redirect the adjacent flame inward and upward. The numerical simulation reveals two main flow patterns, characterized by the predominance of one flame over the other. The process is likely to be cyclic, depending on when the conditions for early flame ignition are met.

With the target of identifying the necessary design modifications to stabilize the flame containing hydrogen, Table 1 presents the percentage variations of the main quantities measured at the burner outlet for the 30 % hydrogen case compared to the baseline configuration.

It is important to note that in the case of a fuel mixture with hydrogen, the presence of this element enriches the low heating value of the fuel. Consequently, a different fuel mass flow rate is required to achieve the same thermal power input as in the baseline case. Moreover, since hydrogen is the lightest element in nature, a reduction of nearly 50 % in the density of the fuel mixture was observed compared to the baseline case. Combining these two factors, an increase of almost 75 % in the velocity of the fuel jet was quantified, assuming that the burner diameter remained unchanged. Considering these new characteristics of the hydrogen-enriched fuel, a key design aspect involves increasing the burner cross-sectional area (the diameter) to reduce the velocity of the fuel jet to values comparable to those in the baseline case.

Table 1
Percentage variations of the main quantities measured by the burners in the 30 % hydrogen case compared to the baseline.

Case	$\dot{m}_{fuel}$ [kg/s]	ρ_{fuel} [kg/m3]	u_{fuel} [m/s]
H_2 30 %	−18.1 %	−52.9 %	+73.2 %

Based on the previous considerations, the first strategy identified to achieve a more stable flame structure is to redesign the burner to ensure consistent fuel velocities with the new fuel mixture. Thanks to the conical shape of the burner ports, burners can be quickly replaced or interchanged, including with different diameters, without requiring a furnace shutdown, which makes changes or upgrades economically efficient and minimizes production downtime. Fig. 7 shows the volume rendering of OH mass fraction for the hydrogen-enriched case with an increased burner diameter, compared to the baseline case.

This modification demonstrates the potential to mitigate the instabilities observed in the original hydrogen-enriched configuration by slowing down the fuel jet and promoting a more stable flame structure. Specifically, it is evident that increasing the nozzle diameter restores the flame structure to a condition like the baseline case (i.e., the configuration using natural gas only, but with smaller nozzle diameters). In both cases, the flames exhibit comparable length and width; moreover, the scenario with the two main flame patterns with the distorted flames is no longer observed. In the configuration with the increased nozzle diameter, ignition was observed to be delayed compared to the hydrogen-enriched case with the original burner configuration. This delay results in flame velocities comparable to those of the baseline case. As a result, the exhaust gases no longer alter the structure of the adjacent flame. This adjustment not only aligns the hydrogen-enriched configuration more closely with the baseline, but it also increases the flame stability. The ability to stabilize the flame by optimizing burner geometry highlights the importance of adapting the design to account for the specific physical and chemical properties of hydrogen-enriched fuel mixtures, such as higher jet velocities and earlier ignition.

A further important aspect to consider is the operating condition at which the furnace is working. In the cases already presented, λ (the actual air fuel ratio to the stoichiometric air fuel ratio) is 0.94; it means that the furnace is operating under fuel-rich conditions with a deficit of air. Under these conditions, in the case of a hydrogen-enriched mixture and unmodified burners, one of the two flames results predominant on the other. It has been observed that when one flame becomes predominant, the adjacent weaker flame receives less oxygen, hindering its

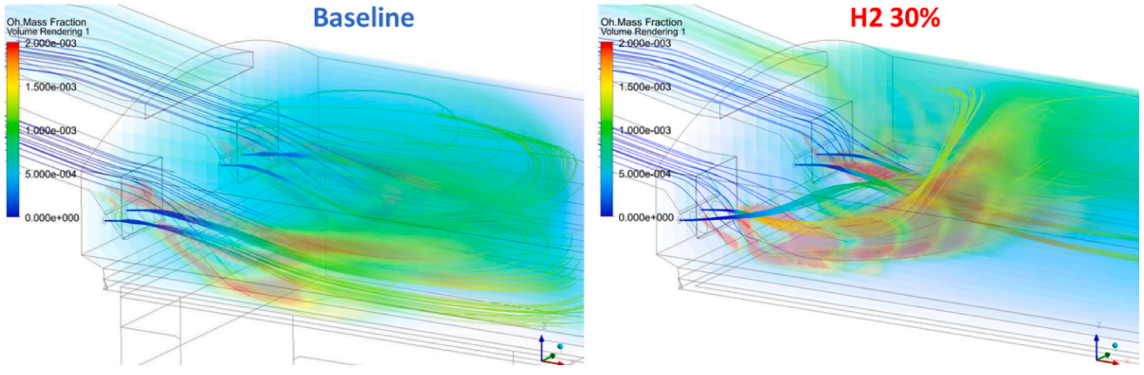

Fig. 6. Zoomed view in the mixing zone of streamlines in the combustion chamber originating from the air ports and burners, along with OH volume rendering, comparing the baseline case (on the left) and the 30 % H_2 case (on the right).

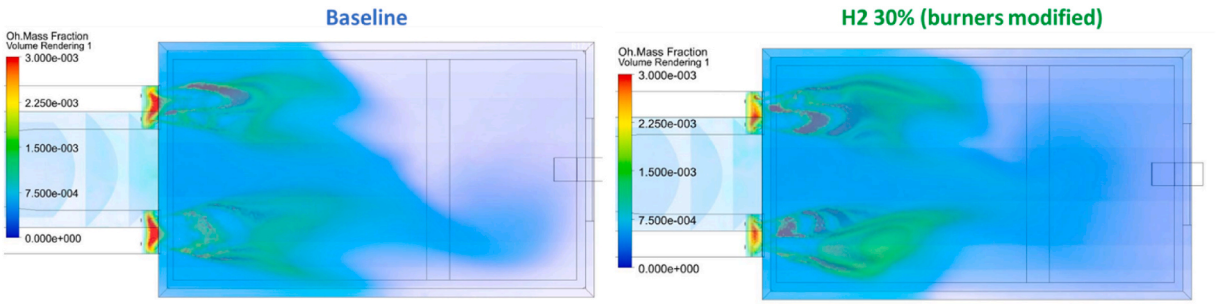

Fig. 7. Comparison of OH volume rendering in the combustion chamber between the baseline case (on the left) and the 30 % H_2 case with modified burners (on the right).

optimal development. Based on this observation, a second design strategy to stabilize the flame structure, without modifying the burner geometry, can be to operate with an air surplus, increasing the air mass flow rate from the corresponding vents. To explore this approach, an analysis was conducted for the hydrogen-enriched case with unmodified burners, by varying the air mass flow rate. Fig. 8 shows the volume rendering of OH mass fraction for various operating conditions.

The analysis reveals that operating with an air surplus, even without modifying the burner geometry, can result in a stable flame configuration. For instance, in the case with $\lambda = 1.10$ (excess of air), two parallel flames are observed, resembling the baseline configuration. This contrasts sharply with the hydrogen-enriched case operating under fuel-rich conditions. By providing more oxygen, both flames can develop along their respective axes without one "suffocating" the other. Consequently, a flow structure is established in which the combustion products, as they move toward the exhaust tower, minimally affect the flame structures. This beneficial effect becomes increasingly evident when operating with a significant air surplus. However, as the system approaches stoichiometric conditions, the flames tend to destabilize again. This phenomenon is observed in the case of $\lambda = 1.05$, where the right-hand flame exhibits slight distortion inward. This suggests that, while working with an air surplus can mitigate flame instability, sufficient margins of excess air are necessary to ensure consistently stable combustion.

In summary, it has been observed that the introduction of hydrogen in the fuel can significantly impact the flame structure, which in this glass furnace exhibits a particular and specular flow pattern compared to the configuration using only natural gas. The analyses conducted have demonstrated that there are two possible strategies to restore the flames to a stable behaviour similar to the baseline case. The first involves increasing the burner diameter to reduce the velocity of the fuel jet to values comparable to those in the baseline configuration. Alternatively, the operating point of the furnace can be adjusted by working with a sufficient margin of excess oxygen. This ensures an adequate oxygen supply for both flames, preventing potential disruptions or "suffocation" of one flame by the other. Further analyses will be presented to study in greater detail the potential impacts on furnace operation and, consequently, on the glass melt, focusing on the most significant cases.

5.3. Comparisons

The cases considered for the subsequent analyses include the following: the baseline case, the case with 30 % hydrogen introduction (without furnace design modifications compared to the baseline) and the two hydrogen-enriched cases incorporating the proposed design modifications from the previous analysis, i.e. burners modification and operational point variation.

First, the numerical model developed with this chemical kinetic mechanism enabled a precise evaluation of the chemical compositions at the combustion chamber exit. The exhaust compositions provide data on primary pollutant emissions, including NO, allowing for a comparison of emissions across the different cases. Table 2 presents the percentage variations in the exhaust gas composition at the outlet for the analyzed

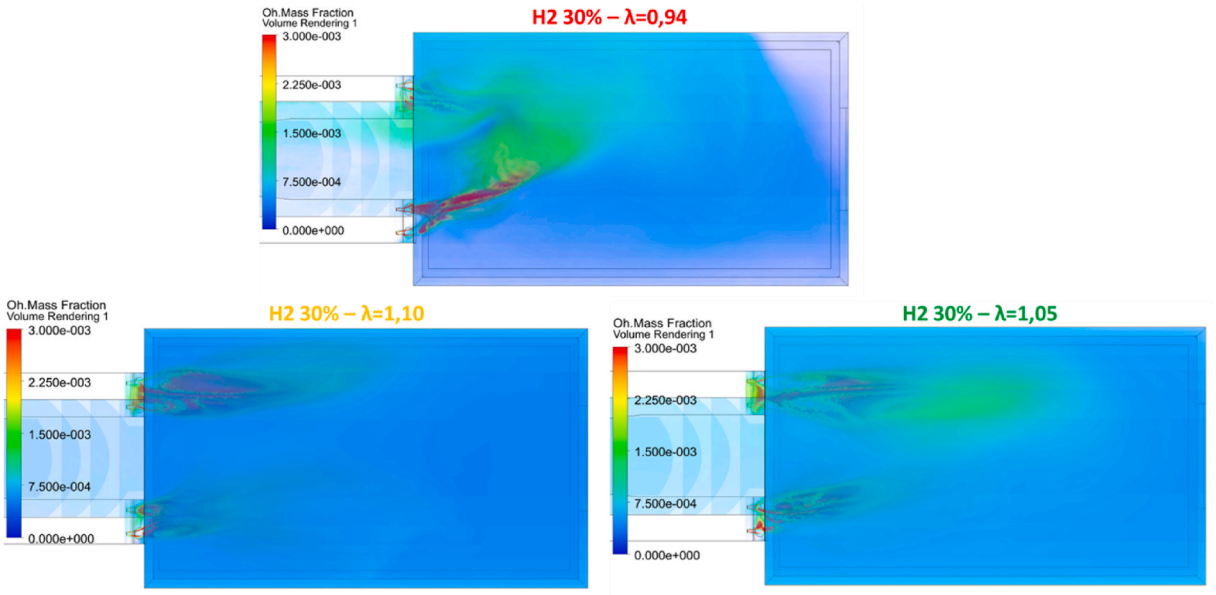

Fig. 8. Comparison of OH volume rendering in the combustion chamber for the 30 % H_2 case under different air mass flow rate.

Table 2
Percentage variations of the main pollutant emissions compared to the baseline case for the most significant hydrogen cases.

Species	H_2 30 % $\lambda = 0,94$	H_2 30 % (burners modified) $\lambda = 0,94$	H_2 30 % $\lambda = 1,10$
O_2	−37,5 %	+167 %	+702 %
CO_2	−28,4 %	−29,8 %	−38,3 %
H_2O	+24 %	+18,6 %	+4,4 %
CO	−4,4 %	−91,8 %	−96 %
NO	−39,5 %	−17,7 %	+249 %

cases, relative to the baseline.

As starting point, it is essential to analyse the oxygen content remaining in the combustion products, as a primary indicator of the combustion completeness. The hydrogen-enriched case with a reduced combustion stability (H_2 30 % $\lambda = 0,94$) exhibits a reduction in the oxygen content in the exhaust gases. This suggests a higher degree of combustion completeness, albeit with distorted flame structures. Conversely, in the case of modified burners (with an increased cross-section and reduced jet velocity), the mixing between fuel and oxidizer, as well as the autoignition process, are affected. As a result, higher oxygen concentrations are observed in the exhaust gases, indicating a less complete combustion process. As a result, a portion of the injected oxygen remains unreacted in the flue gases. Despite this, the modified burner geometry facilitates the formation of parallel flame structures, as the increased availability of oxidizer promotes flame stabilization across a broader region of the furnace. Additionally, in the hydrogen-enriched case without burner modifications but with an air-surplus operating point, a significant increase in oxygen content in the exhaust gases is observed; it is directly attributed to the higher air mass flow entering through the air vents. In this latter case, despite the high velocity of the fuel jet, the abundance of oxygen prevents either flame from being "suffocated."

Regarding carbon monoxide (CO) emissions, a significant reduction is observed across all cases compared to the baseline, particularly in the cases with modified burners and with excess air. This reduction occurs because the increased availability of oxygen enhances the completion of the reaction, favouring the formation of CO_2 over CO.

Nitrogen oxide (NO) emissions exhibit a complex behaviour that depends on both the fuel composition and the furnace operating conditions. In the hydrogen-enriched case without burner modifications, NO emissions are markedly reduced. This reduction primarily arises from the more complete combustion, which decreases the local availability of oxygen within the reaction zones. Additionally, the flames under these conditions appear narrower (as shown in Fig. 4), leading to smaller hot-spot regions and consequently, a lower rate of NO formation. According to the Zeldovich mechanism, NO generation is initiated in high-temperature regions, moreover a reduction in local O_2 concentration effectively limits the NO production pathway [61,68]. Conversely, when burner geometry is modified (with the increased nozzle diameter) to better accommodate the hydrogen-enriched mixture, NO emissions remain low despite locally higher oxygen concentrations. In this configuration, the dominant factor is the reduction in combustion hotspots, mainly due to less complete local combustion, which limits the onset of the Zeldovich mechanism, initiated by O_2 dissociation. In contrast, in cases with excess air, the substantial higher oxygen availability promotes NO formation. From an industrial perspective, these trends have important implications. Lower NO emissions contribute to compliance with environmental regulations and reduce the need for downstream emission control measures. Moreover, controlling hotspot formation can be beneficial not only for emission reduction but also for product quality, as extreme local temperatures can affect glass homogeneity.

Finally, analysing the carbon dioxide (CO_2) and water vapor (H_2O) content in the flue gases reveals a substantial reduction in CO_2, one of the primary greenhouse gases, across all three hydrogen-enriched cases compared to the baseline. This is due to the use of a fuel with a lower carbon content, combined with an increased presence of water vapor, which results from the higher hydrogen content in the fuel.

An additional advantage of the developed CFD model, achieved through the full coupling of the combustion space and the glass tank, is its ability to assess the responses of the glass bath's free surface under various scenarios. Fig. 9 illustrates the heat flow distributions on the free glass surface for the considered cases.

The footprint of the flames on the free glass surface is clearly well visible, extending across approximately half the length of the bath. Additionally in all cases, the doghouse region on the right (where glass enters at ambient temperature) can be observed to absorb a significant amount of heat flow from the combustion space. This is consistent with the energy requirements of the entering glass to reach the necessary fusion temperature.

In most cases, the flame imprints on the free glass surface appear parallel, reflecting the parallel flame structures in the combustion space. However, an exception is noted in the hydrogen-enriched case with unmodified burners and the original operating condition (with air-defect). In this scenario, consistent with the previously observed flame patterns, the phenomenon of a dominant flame (here the left flame) and the adjacent flame tilted toward it leads to a noticeably more asymmetrical heat flow distribution.

In addition, it is also crucial to quantify the average heat flow that is transferred from the combustion space to the glass bath. Table 3 presents the percentage variations of the averaged main contribution to the power balance for each scenario, compared to the baseline case.

Q_{fuel} is the product of the fuel mass flow rate and the corresponding low heating value, while $Q_{to\text{-}glass}$ is the heat flow from the combustion chamber, predominantly due to thermal radiation Initially, it can be seen that, in comparison to the baseline case, Q_{fuel} for the hydrogen-enriched mixture shows a slight increase in the scenario with any modifications on the furnace. This increase is attributed to the more complete combustion process, even though the flames have a reduced stability. This suggests that the combustion with hydrogen, is slightly more efficient in terms of energy produced than the baseline. In contrast, the two other cases with design modifications (burner modifications or operational point changes) show a modest reduction in Q_{fuel}. This reduction is due to a less complete combustion process, which is consistent with the results observed in the pollutant emissions analysis. The less efficient combustion in these cases means less energy is being produced, which impacts the overall performance of the furnace in terms of heat flow.

Consistent with the observed variations for Q_{fuel}, the heat flow from the combustion chamber transferred to the underlying glass bath shows similar patterns. In the hydrogen case without any design modifications, the heat flow transferred to the glass is slightly increased. This is likely due to the higher efficiency in energy generation, albeit with a less stable flame structure. On the other hand, in the two cases where modifications were made (burner or operating point), a slight decrease in the heat flow to the glass is observed. This is again in line with the reduction in Q_{fuel}, suggesting that a less complete combustion process results in a lower overall energy transferred to the free glass surface.

Fig. 10 displays the temperature distributions on the free glass surface for the different cases. They show the temperature spatial variation along the free glass surface under different conditions, allowing for a clear comparison among cases.

There is a perfect match between the temperature peaks on the glass and the maxima heat flow observed in the previous representation. This correlation is a unique feature allowed by the full thermal coupling between the combustion space and the glass bath, ensuring that both the heat flow and temperature distributions are accurately reflected and interrelated rather than traditional models reported in literature. The temperature peaks are located just before the middle of the furnace, with the flame imprints appearing nearly parallel in all the cases, except for the scenario with a distorted flame (30 % H_2, $\lambda = 0.94$). In this last case,

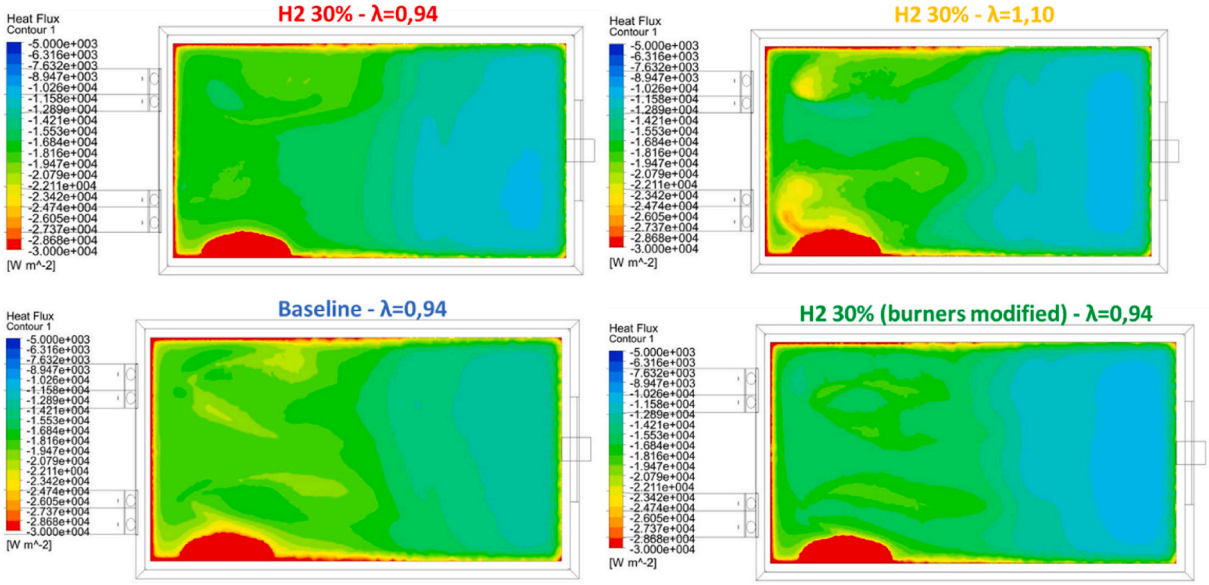

Fig. 9. Comparison of the heat flow on the free glass surface between the main cases analyzed.

Table 3
Percentage variations of the main contributions to the power balance compared to the baseline case for the most significant hydrogen cases.

Heat flow contributions	H_2 30 % $\lambda = 0,94$	H_2 30 % (burners modified) $\lambda = 0,94$	H_2 30 % $\lambda = 1,10$
Q_{fuel}	+2,7 %	−5,8 %	−3,6 %
$Q_{to\text{-}glass}$	+4,3 %	−1,4 %	−0,8 %

a marked longitudinal asymmetry in the heat flow and temperature distribution is observed, because the dominant flame (the left one) causes the heat flow to concentrate more on that side of the glass. This behaviour in the flame structure, caused by the hydrogen mixture and the air-defect operating condition, leads to this irregular distribution pattern. Such asymmetry may negatively affect the homogenization of the molten glass, which is a fundamental design requirement for glass manufacturers.

In addition, the temperatures on the free glass surface are slightly lower in the cases where design modifications were made. This is because the combustion process in these modified cases is less complete, resulting in lower reaction heat and consequently less energy transferred to the glass bath. The decrease in heat flow leads to a lower temperature on the glass surface compared to the baseline, where the combustion process is more complete and the energy released is higher. The design modifications, although stabilizing the flame, also result in a more controlled and less intense heat transfer to the glass, which can have a good impact the glass production process.

6. Conclusions

In this work, an advanced CFD model was developed to simulate the operation of an industrial glass production furnace. The first key innovation lies in the use of a detailed multispecies combustion model, solving the reactive flow with a reduced chemical kinetic scheme

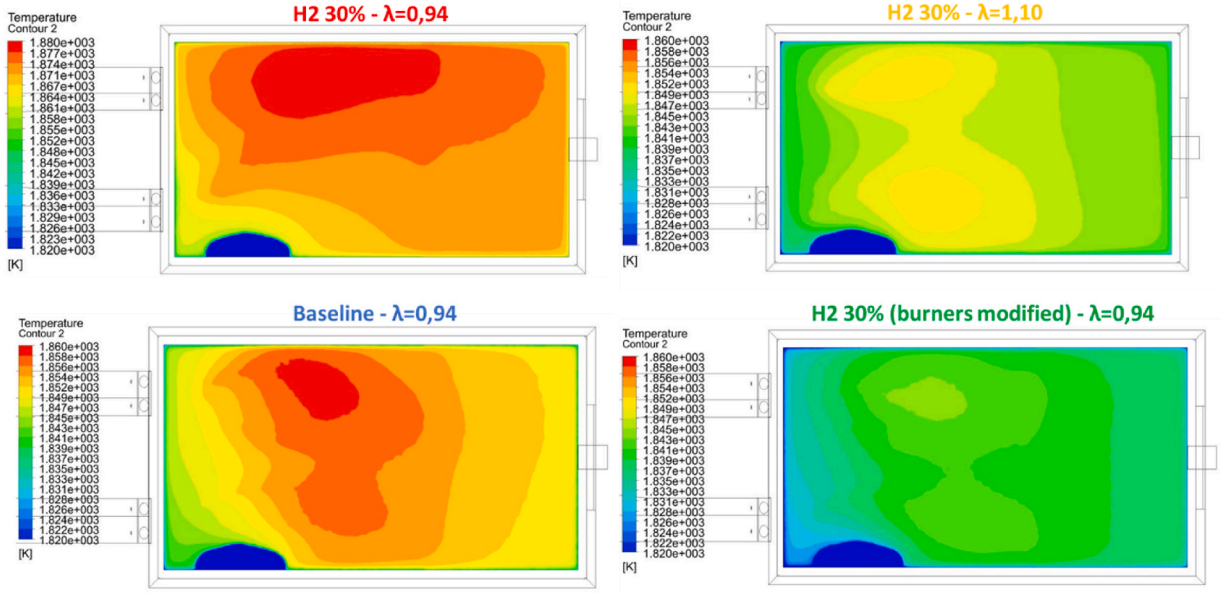

Fig. 10. Comparison of the static temperature on the free glass surface between the main cases analyzed.

derived from GriMech and coupled with the Eddy Dissipation Concept (EDC) to accurately capture turbulence–chemistry interactions — overcoming the limitations of simplified approaches typically used in literature. The second major advancement is the implementation of a fully integrated thermal coupling between the combustion space and the glass bath. Unlike conventional models, which solve the two domains separately and connect them through iterative boundary exchanges, the present model resolves both regions simultaneously within a single computational framework. This enables consistent prediction of heat transfer across the interface and reveals its direct influence on the convective motion within the molten glass.

A specific focus of the study was to evaluate the impact of introducing 30 % hydrogen into the fuel mixture, while maintaining the same total thermal power as the baseline case using only natural gas. The aim was to understand how hydrogen affects flame structures and more broadly the furnace performance. The results indicated that hydrogen addition, in this glass plant, tends to reduce the combustion stability. Specifically, two main, specular flame patterns have been identified, with one flame consistently predominant over the other, which appears weaker and more distorted. This leads to an asymmetrical heat distribution at the molten glass surface, potentially compromising the quality of the final product.

Through a detailed fluid dynamic analysis, two effective strategies were identified to restore flame stability in the presence of hydrogen:

- Adjusting the burner diameter to achieve jet velocities comparable to the baseline case with natural gas;
- Operating with at least 10 % excess air, to prevent flame quenching and promote a more stable combustion regime.

Furthermore, the simulations enabled a quantitative evaluation of the benefits of hydrogen enrichment relative to the baseline configuration, considering both the original and modified burner designs. With the same equivalent ratio, the addition of hydrogen led to nearly a 30 % reduction in CO_2 emissions, which increased to approximately 40 % when operating with excess air. As for NO emissions, a strong reduction was also observed in the hydrogen-enriched cases; this improvement was observed in the cases operating at the same low air–fuel ratio as the baseline configuration.

The primary objective of this work was to explore the potential for decarbonization in the glass industry with a sophisticated CFD model capable of simulating realistic furnace behaviour with alternative fuels. By focusing on hydrogen as a clean energy carrier, the study aimed to identify feasible and practical strategies that can support the industry's transition toward low-carbon technologies. This model serves as a powerful tool for future parametric analyses, enabling optimization of both fuel composition and furnace geometry and ultimately contributing to the broader goal of improving energy efficiency for reducing emissions in industrial glass production.

CRediT authorship contribution statement

Carlo Cravero: Writing – review & editing, Supervision, Resources, Project administration, Methodology, Investigation, Funding acquisition, Conceptualization. **Davide Marsano:** Writing – original draft, Visualization, Validation, Software, Resources, Methodology, Investigation, Formal analysis, Data curation, Conceptualization. **Gabriele Milanese:** Writing – original draft, Visualization, Validation, Software, Resources, Methodology, Investigation, Formal analysis, Data curation, Conceptualization.

Funding

This research was developed within the project "Network 4 Energy Sustainable Transition—NEST" funded under the National Recovery and Resilience Plan (NRRP); and the Mission 4 Component 2 Investment 1.3—Call for tender No. 1561 of 11.10.2022 of Ministero dell'Università e della Ricerca (MUR), funded by the European Union#8212; NextGenerationEU.

Declaration of competing interest

The authors declare that they have no known competing financial interests or personal relationships that could have appeared to influence the work reported in this paper.

Acknowledgments

The research activity carried out by the University of Genoa research group was conducted on a glass furnace configuration provided by Bormioli Pharma S.p.A., whose support is gratefully acknowledged. The research team from the University of Genova is grateful to the technical group of Bormioli Pharma for their support in the discussion of the complex topics involved in this paper and for the welcome opportunity to work on this very specific and difficult application.

Nomenclature

FP	Flame topology
J_n	Diffusion flux of species n
K	Turbulent kinetic energy
L	Length
$\dot{m}$	Mass flow rate
Q	Power
R_n	Net rate of production of species n
S_{ij}	Rate of strain tensor
t	Time
T	Temperature
u	Velocity
x	Cartesian coordinate
Y_n	Mass fraction of species n
γ^*	Length scale
ε	Rate of dissipation of turbulent kinetic energy
ε_v	Thermal emissivity
λ	Actual air fuel ratio to the stoichiometric air fuel ratio
μ	Dynamic viscosity
μ_t	Turbulent viscosity
ν	Kinematic viscosity

(*continued on next page*)

(*continued*)

ρ	Density
τ^*	Mean residence time
Subscript	
cor	Corrected

References

[1] GlassGlobal [Internet]. [cited 2023 Jul 21]. Available from: https://www.glassglobal.com/.
[2] European Climate, Infrastructure and Environment Executive Agency. How LIFE is reducing emissions from glass production. 2022.
[3] Atzori D, Tiozzo S, Vellini M, Gambini M, Mazzoni S. Industrial technologies for CO2 reduction applicable to glass furnaces. Thermo 2023;3:682–710.
[4] Un green deal europeo. Available online: https://commission.europa.eu/strategy-and-policy/priorities-2019-2024/europeangreen-deal_it.
[5] Koshelnik AV. Modelling operation of system of recuperative heat exchangers for aero engine with combined use of porosity model and thermos-mechanical model. Glass Ceram 2008;65(9–10):301–4.
[6] Zier M, Stenzel P, Kotzur L, Stolten D. A review of decarbonization options for the glass industry. Energy Convers Manag X 2021;10(February):100083.
[7] Selvaray J, Varun VS, Vishwam V. Waste heat recovery from metal casting and scrap preheating using recovered heat. Procedia Eng 2014;97:267–76.
[8] Fathi M, Saray RK, Checkel MD. The influence of Exhaust Gas Recirculation (EGR) on combustion and emissions of n-heptane/natural gas fueled homogeneous charge compression ignition (HCCI) engines. Appl Energy 2011;88:4719–24.
[9] Spliethoff H, Greul U, Rüdiger H, Hein KR. Basic effects on NOx emissions in air staging and reburning at a bench-scale test facility. Fuel 1996;75:560–4.
[10] Staiger B, Unterberger S, Berger R, Hein KR. Development of an air staging technology to reduce NOx emissions in grate fired boilers. Energy 2005;30:1429–38.
[11] Guillen DP. Bubbling behavior in a waste glass melter. WIT Trans Eng Sci 2016;105:75–85.
[12] Kuzyak VA. Electric boosting of glass heating in flame tank furnaces. Glass Ceram 1958;15:586–91.
[13] He K, Wang L. A review of energy use and energy-efficient technologies for the iron and steel industry. Renew Sustain Energy Rev 2017;70:1022–39.
[14] Liu W, Zuo H, Wang J, Xue Q, Ren B, Yang F. The production and application of hydrogen in steel industry. Int J Hydrogen Energy 2021;46:10548–69.
[15] Gołdasz A, Matuszewska D, Olczak P. Technical, economic, and environmental analyses of the modernization of a chamber furnace operating on natural gas or hydrogen. Int J Hydrogen Energy 2022;47(27):13213–25.
[16] "HyGlass | IN4climate.NRW". https://www.in4climate.nrw/best-practice/2020/hyglass/. [Accessed 6 November 2020].
[17] "NSG to test hydrogen fuel for glassmaking at St Helens site", Glass Int. https://www.glass-international.com/news/nsg-to-use-hydrogen-fuel-for glassmaking-at-st-helens-site (November 2020).
[18] Kopernikus projekte: Kopernikus-Projekt: P2X. https://www.kopernikusprojekte.de/projekte/p2x (Nov. 06, 2020).
[19] Chae MJ, Kim JH, Moon B, Park S, Lee YS. The present condition and outlook for hydrogen-natural gas blending technology. Korean J Chem Eng 2022;39:251–62.
[20] Lee S-W, Lee H-S, Park Y-J, Cho Y-S. Combustion and emission characteristics of HCNG in a constant volume chamber. J Mech Sci Technol 2011;25:489–94.
[21] Ozturk M, Sorgulu F, Javani N, Dincer I. An experimental study on the environmental impact of hydrogen and natural gas blend burning. Chemosphere 2023;329:138671.
[22] Capurso T, Ceglie V, Fornarelli F, Torresi M, Camporeale SM. CFD analysis of the combustion in the BERL burner fueled with a hydrogen-natural gas mixture. E3S Web Conf 2020;197:10002.
[23] Stefanizzi M, Stefanizzi S, Ceglie V, Capurso T, Torresi M, Camporeale SM. Analysis of the partially premixed combustion in a labscale swirl-stabilized burner fueled by a methane-hydrogen mixture. E3S Web Conf 2021;312:11004.
[24] Ziani L, Chaker A, Chetehouna K, Malek A, Mahmah B. Numerical simulations of non-premixed turbulent combustion of CH4–H2 mixtures using the PDF approach. Int J Hydrogen Energy 2013;38:8597–603.
[25] Bouziane A, Alami A, Zaitri M, Bouchame B, Bouchetara M. Investigation of swirl stabilized CH4 air flame with varied hydrogen content by using computational fluid dynamics (CFD) to study the temperature field and flame shape. Eng Technol Appl Sci Res 2021;11:6943–8.
[26] Cellek MS, Pınarbaşı A. Investigations on performance and emission characteristics of an industrial low swirl burner while burning natural gas, methane, hydrogen-enriched natural gas and hydrogen as fuels. Int J Hydrogen Energy 2018;43:1194–207.
[27] McConnell RR, Goodson RE. Modeling of glass furnace design for improved energy efficiency. Glass Technol 1979;20:100–6.
[28] Mase H, Oda K. Mathematical model of glass tank furnace with batch melting process. J Non-Cryst Solids 1980;38–39:807–12.
[29] Carvalho MG. Computer simulation of a glass furnace. London, UK: London University; 1983. PhD Thesis.
[30] Carvalho MG, Lockwood FC. Mathematical simulation of an end-port regenerative glass furnace. Proc Inst Mech Eng C 1985;199:113–20.
[31] Carvalho MG, Oliveira P, Semiao V. A three-dimensional modelling of an industrial glass furnace. J Inst Energy 1988;61:143–56.
[32] Carvalho MG, Nogueira M. Modelling fluid flow and heat transfer in an industrial glass furnace. In: Proceedings of the annual ESPRIT conference; 1990. p. 530–43. Dordrecht, The Netherlands.
[33] Carvalho MG, Nogueira M. Modelling of glass melting industrial process. J Phys 1993;IV:1357–66.
[34] Carvalho MG, Nogueira M, Wang J. Mathematical modeling of glass melting industrial process. Proceedings of the 17th International Congress on Glass 9–14 October 1995;6:69–74. Beijing, China.
[35] Chmelar J, Schill P, Franek A. Mathematical models of glass melting furnaces. In: Proceedings of the 4th international conference on advances in fusion and processing of glass. Germany: Wurzburg; 22–24 May 1995. p. 63–6.
[36] Hoke BC, Marchiando RD. Using combustion modeling to improve glass melt model results. In: Proceedings of the 4th In-ternational seminar on mathematical simulation in the glass melting. Horni Becva, Czech Republic; 1997. p. 87–95.
[37] Golchert B, Zhou CQ, Chang SL, Petrick M. Investigation of spectral radiation heat transfer and NOx emission in a glass furnace. In: Proceedings of the international mechanical congress and exposition; November 2000. p. 5–10. Orlando, FL, USA.
[38] Chang SL, Zhou CQ, Golchert B. Eulerian approach for multiphase flow simulation in a glass melter. Appl Therm Eng 2005;25:3083–103.
[39] Wang J, Brewster BS, Mcquay MQ, Webb BW. Validation of advanced models for glass melting furnaces. In: Proceedings of the 60th conference on glass problems; October 2000. p. 19–20. Urbana, IL, USA.
[40] Abbassi A, Khoshmanesh K. Numerical simulation and experimental analysis of an industrial glass melting furnace. Appl Therm Eng 2008;28:450–9.
[41] Li L, Lin HJ, Han J, Ruan J, Xie J, Zhao X. Three-dimensional glass furnace model of combustion space and glass tank with electric boosting. Mater Trans 2019;60:1034–43.
[42] Raič J, Gaber C, Wachter P, Demuth M, Gerhardter H, Knoll M, Prieler R, Hochenauer C. Validation of a coupled 3D CFD simulation model for an oxy-fuel cross-fired glass melting furnace with electric boosting. Appl Therm Eng 2021;195:117166.
[43] Daurer G, Raič J, Demuth M, Gaber C, Hochenauer C. Detailed comparison of physical fining methods in an industrial glass melting furnace using coupled CFD simulations. Appl Therm Eng 2023;232:121022.
[44] Cravero C, Marsano D. Numerical simulation of regenerative chambers for glass production plants with a non-equilibrium heat transfer model. WSEAS Trans Heat Mass Transf 2017;12:21–9.
[45] Cravero C, De Domenico D, Leutcha PJ, Marsano D. Strategies for the numerical modelling of regenerative pre-heating systems for recycled glass raw material. Math Model Eng Probl 2019;6:324–32.
[46] Cravero C, De Domenico D, Marsano D. The use of uncertainty quantification and numerical optimization to support the design and operation management of air-staging gas recirculation strategies in glass furnaces. Fluids 2023;8:76.
[47] Cravero C, Marsano D. Numerical simulation of melted glass flow structures inside a glass furnace with different heat release profiles from combustion. Energies 2023;16:4187.
[48] Cravero C, Lamberti A, Marsano D, Milanese G. Numerical investigation of turbulent fuel jet diffusion and its influence on the auto-igniting diffusive flame development. J Phys Conf Ser 2024;2893:012032.
[49] Cravero C, Marsano D, Milanese G. CFD simulation of the increased electric boost effects on the glass melting process in a real glass furnace to support decarbonisation of glass industry. J Phys Conf Ser 2024;2893:012033.
[50] Cravero C, Marsano D, Milanese G. A CFD model for the direct coupling of the combustion process and glass melting flow simulation in glass furnaces. Energies 2025;18:1792.
[51] Launder BE, Spalding DB. Mathematical models of turbulence. London, UK: Academic Press; 1972.
[52] Rodi W. Turbulence models and their application in hydraulics. IAHR monograph series; A state-of-the-art review. third ed. Rotterdam, The Netherlands: A.A. Balkema; 2017.
[53] Gran IR, Magnussen BF. A numerical study of a bluff-body stabilized diffusion flame. Part 2. Influence of combustion modeling and finite-rate chemistry. Combust Sci Technol 1996;119:191–217.
[54] Launder BE, Spalding DB. The numerical computation of turbulent flows. Comput Methods Appl Mech Eng 1974;3:269–89.
[55] Thangam S. Analysis of two-equation turbulence models for recirculating flows; NASA/CR-1991-187607. Available online: https://ntrs.nasa.gov/citations/19910021161.
[56] Magnussen B. On the structure of turbulence and a generalized eddy dissipation concept for chemical reaction in turbulent flow. In: Proceedings of the 19th aerospace sciences meeting, aerospace sciences meetings. St. Louis, MO, USA: American Institute of Aeronautics and Astronautics; January 1981. p. 12–5.

[57] Modest M. Radiative heat transfer. second ed. Cambridge, MA, USA: Academic Press; 2003.
[58] Peters N. Laminar diffusion flamelet models in non-premixed turbulent combustion. Prog Energy Combust Sci 1984;10:319–39.
[59] Available online: http://combustion.berkeley.edu/gri_mech/. [Accessed 31 May 2025].
[60] Skjøth-Rasmussen MS, Holm-Christensen O, Østberg M, Christensen TS, Johannessen T, Jensen AD, Glarborg P, Livbjerg H. Post-processing of detailed chemical kinetic mechanisms onto CFD simulations. Comput Chem Eng 2004;28 (11):2351–61.
[61] Cuoci A, Frassoldati A, Stagni A, Faravelli T, Ranzi E, Buzzi-Ferraris G. Numerical modeling of NO x formation in turbulent flames using a kinetic post-processing technique. Energy & Fuels 2013;27(2):1104–22.
[62] Stagni A, Cuoci A, Frassoldati A, Faravelli T, Ranzi E. A fully coupled, parallel approach for the post-processing of CFD data through reactor network analysis. Comput Chem Eng 2014;60:197–212.
[63] Mavris D. Enhanced emission prediction modeling and analysis for conceptual design. Final Report for NASA grant NNX07AO08A 2010;17.
[64] ANSYS Inc. Ansys fluent theory guide v.17. Canonsburg, PA, USA: ANSYS Inc.; 2017.
[65] Davoudzadeh F, Liu NS, Moder JP. Investigation of swirling air flows generated by axial swirlers in a flame tube. Turbo Expo Power Land Sea Air 2006;42363: 891–902.
[66] Rahman TMR. An investigation of RANS simulations for swirl-stabilized isothermal turbulent flow in a gas turbine burner. CFD Lett 2019;11:14–31.
[67] Sommariva B. Development of a CFD reactive model for combustion simulation in glass furnace. University of Genoa; 2024. Master Thesis.
[68] Mullinger P, Jenkins B. Industrial and process furnaces: principles, design and operation. Butterworth-Heinemann; 2022.